presented at Mini Workshop on Applied Mathematics, Sylhet, Bangladesh, September 1998

UNSTEADY AXISYMMETRIC FLOW IN A ROTATING CAVITY WITH A STATIONARY OUTER SURFACE

T. W. Lewis, D. A. S. Rees and M. Wilson

Department of Mechanical Engineering
Faculty of Engineering and Design
University of Bath
Bath BA2 7AY
United Kingdom

ABSTRACT

Unsteady axisymmetric solutions of the Navier−Stokes equations have been obtained, using the vorticity−streamfunction formulation, for the flow in a rotating cavity with a stationary outer casing. The secondary flow is characterised by counter−rotating vortices in the outer part of the system, with radial inflow near the mid−plane between the co−rotating discs. Computed tangential velocity distributions follow Rankine (combined free and forced) vortex distributions, and are in reasonable agreement with available experimental data. Comparisons are also made between the results of the unsteady computations and steady flow results obtained using a two−equation low Reynolds number turbulence model.

1 INTRODUCTION

The rotating cavity illustrated in Fig. 1, formed by co−rotating discs separated by a rotating inner cylinder (or hub), and with a stationary outer casing, has been studied in relation to two practical engineering situations. Abrahamson et al (1989) described an experimental study carried out in order to provide information on the air flow in computer disc drives, and Chang et al (1990) also carried out axisymmetric, steady calculations for this application. Gan et al (1996) and Mirzaee et al (1997) carried out experiments and computations for flow and heat transfer in a similar rotating cavity, using this as a simplified model for co−rotating turbine discs in a gas−turbine engine. A comprehensive review of flow and heat transfer in rotating cavities is given by Owen and Rogers (1995).

Gan et al (1996) made laser−Doppler anemometry (LDA) velocity measurements, and carried out steady turbulent flow computations (using a low Reynolds−number k−ε turbulence model for the Reynolds−averaged Navier−Stokes equations), for a rotating cavity with a/b = 0.5 and gap ratio G = s/b= 0.3 (see Fig. 1). The range of rotational Reynolds numbers tested was $1.5 \times 10^5 < Re_\phi < 1.5 \times 10^6$.

In addition to the flow due to the stationary casing, Gan et al (1996) also investigated the effect of a peripheral flow of air, simulating the flow used to cool gas−turbine discs. Heat transfer for these "superposed flow" cases was measured and computed by Mirzaee et al (1997).

Abrahamson et al (1989) carried out flow visualisation in a similar rotating cavity to that described above, again with a/b = 0.5, but with the axial spacing between the discs varied so that $0.013 < G < 0.1$. The range of rotational Reynolds numbers studied was the same as that considered by Gan et al. Orderly circumferential asymmetries were observed in the flow, with a number of vortices in the outer part of the cavity precessing relative to the discs. Near solid−body rotation occurred in the inner region towards the hub. The number of vortices decreased (and the level of relative motion in the inner region increased) when the axial separation between the discs was increased. Ensemble−averaged tangential velocities on the mid−plane between the discs (inferred from flow visualisation results) were presented for $Re_\phi = 4.5 \times 10^5$ and G = 0.05. These showed a clear distinction between free−vortex−type flow in the outer region, near the casing, and forced−vortex−type flow in the inner part of the cavity.

Fig. 1 shows the secondary flow recirculations for axisymmetric, steady flow computed by Wilson et al (1996), for $Re_\phi = 10^4$ and G = 0.3. The recirculations are symmetric about the axial mid−plane, with radial outflow in the boundary layers on the discs and radial inflow at the mid−plane. (Abrahamson et al (1989) also noted this structure). Gan et al (1996) found, from both experiment and computation, that the inward penetration of these recirculations reduced with increasing rotational Reynolds number. LDA measurements of tangential velocities on the mid−plane (z*/s = ½) followed a Rankine (combined

free and forced) vortex structure, which was not well predicted using the Launder and Sharma (1974) low Reynolds−number k−ε turbulence model. Wilson et al (1997) described results of unsteady axisymmetric computations of the flow (some of this work is reproduced in this paper), and Lewis et al (1997) studied the effect of buoyancy on the stability of the flow, in heat transfer computations carried out at selected conditions.

This paper describes unsteady, axisymmetric, incompressible computations for the flow in the rotating cavity at three conditions, varying both rotational Reynolds number and gap ratio, with comparison against experimental data (where available) and the results of steady flow computations employing "statistical" turbulence models. Section 2 describes the computational method. The results of time−dependent simulations are described and discussed in Sections 3, 4 and 5. Conclusions (and recommendations for future work) appear in Section 6.

2 COMPUTATIONAL METHOD

The Navier−Stokes equations for axisymmetric, incompressible flow, expressed in a rotating frame of reference, were solved in non−dimensional form using the streamfunction−vorticity formulation. This was preferred to the primitive variables formulation in order to overcome the difficulties, associated with the latter, in determining values of pressure at the boundaries. The method also requires around 50% fewer operations than the vorticity−velocity formulation, for which an additional Poisson equation needs to be solved and for which a staggered grid is required in order to obtain divergence−free velocity and vorticity vectors.

The non−dimensional form of the equations is:

$$\frac{\partial\omega}{\partial t} + \frac{\partial\omega}{\partial r}\frac{\partial\Phi}{\partial z} - \frac{\partial\Phi}{\partial z}\frac{\partial\omega}{\partial r} - \frac{1}{r}\left(\Phi\frac{\partial\omega}{\partial z} + \omega\frac{\partial\Phi}{\partial z}\right) - \frac{2\nu}{r}\frac{\partial v}{\partial z} - 2Re_\phi\frac{\partial v}{\partial z} = \nabla^2\omega - \frac{\omega}{r^2} \quad (1)$$

where the vorticity ω is given by $\omega = (\nabla^2\Phi - \Phi / r^2)$, and:

$$\frac{\partial v}{\partial t} + \frac{\partial v}{\partial r}\frac{\partial\Phi}{\partial z} - \frac{\partial\Phi}{\partial z}\frac{\partial v}{\partial r} + \frac{1}{r}\left(v\frac{\partial\Phi}{\partial z} - \Phi\frac{\partial v}{\partial z}\right) + 2Re_\phi\frac{\partial\Phi}{\partial z} = \nabla^2 v - \frac{v}{r^2} \quad (2)$$

For convenience, the streamfunction ψ (which satisfies the continuity equation exactly) has been re−scaled using $\psi = r\Phi$. The non−dimensional variables appearing in the above equation are given from:

$$r^* = br\ ,\ z^* = bz\ ,\ v^* = \nu v/b\ ,\ t^* = b^2t/\nu\ ,\quad w^* = \nu w/b^2\ ,\ \Phi^* = \nu\Phi \quad (3)$$

The rotational Reynolds number, $Re_\phi = \Omega b^2/\nu$, appears only in the Coriolis coupling terms. For the tangential velocity results described below, the absolute velocity was deduced from:

$$V_\phi = v^* + \Omega r^* \quad (4)$$

No−slip conditions apply on the boundaries of the cavity, giving $\Phi = 0$ and zero relative tangential velocity on the boundaries. For the vorticity, $\omega = \partial^2\Phi/\partial r^2$ was

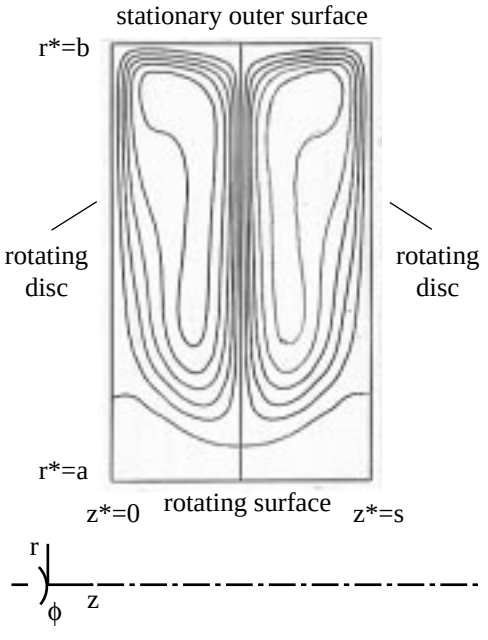

Fig. 1 The rotating cavity, and computed secondary flow streamlines, for steady flow at $Re_\phi = 10^4$

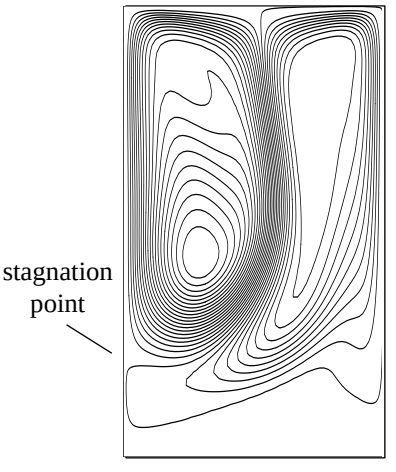

Fig. 2 Instantaneous secondary flow streamlines for unsteady flow computation: $Re_\phi = 10^4$

used at the inner and outer surfaces (at r*=a and r*=b), and $\omega = \partial^2\Phi/\partial z^2$ was used at the surfaces of the two discs (at z*=0 and z*=s).

At high rotational Reynolds numbers, the boundary layers on the rotating discs are thin and a fine grid is required for adequate resolution. Thus, the equations were discretised on a non−uniform mesh in which grid−spacing increased away from solid boundaries as a geometric progression, using expansion factors between 1.1 and 1.2. Uniform spacing (in each direction), matched to this near−wall grid, was used for the mesh in the interior of the cavity.

Hybrid−upwind differencing was used for the non−linear convection terms, in which either second−order accurate central differences, or first−order accurate upwind differences, were used depending upon the local value of the Peclet number Pe = Vh/ν, where V and h represent, respectively, the local velocity and grid−spacing (the appropriate non−dimensional quantities were used within the computational sequence). Further details of the grid, and the results of grid−dependence tests, are given in subsequent sections.

The conditionally−stable, first−order accurate Du−Fort Frankel method was used for the temporal derivatives, in which the dependent variables were averaged between old and new time values. This gave decreased computational expense per time−integration (compared with unconditionally stable methods), and the fixed solution time−step for each different calculation was determined from numerical stability studies.

A fixed V−cycle multigrid algorithm, with line−relaxation smoothing provided by the tri−diagonal matrix algorithm, was used to accelerate the solution of the Poisson equation for the streamfunction. Multigrid convergence at each time−step required the total absolute residual on the mesh to fall below 10^{-6} for the Poisson equation solution (for a case in which the maximum streamfunction value was around 50). Values of vorticity on the boundaries were updated using the streamfunction solution at the new time level. The numerical methods were successfully validated against previously published computational results (for heat transfer) for buoyancy induced flow in differentially heated cavities (in a separate programme of work using this code).

In outline, the solution sequence at each time level is as follows:

i/ solve for ω and v at the new time, using current and old time values, on all internal grid points,

ii/ solve implicitly, using the multigrid method, for Φ at the new time, using the new time values for ω on the right hand side,

iii/ update the boundary values for ω at the new time, using the new time values for Φ

The fluid was initially at rest in the stationary frame of reference, and the rotating surfaces assumed a fixed given speed instantaneously at time t = 0. In order to perturb the solution from a symmetric twin recirculation structure (as ilustrated in Fig. 1), a small axially varying perturbation to the tangential velocity could be introduced. It was found, however, that amplification of round−off errors in the solution was sufficient to perturb the flow, and the results presented here do not include the use of an imposed perturbation.

3 RESULTS FOR $Re_\phi = 10^4$, G = 0.3

Fig. 2 shows instantaneous computed streamlines for unsteady laminar flow in the rotating cavity at $Re_\phi = 10^4$. For this computation, the nondimensional time−step ($\nu\Delta t/b^2$) was around 7×10^{-7}, and an 80 x 96 axial by radial grid was used (b = 0.382 m was used for this case, matching the geometry of the experimental rig in the study referred to in Section 4 below).

The computed flow was periodic, as illustrated in Fig. 3 by the variation with time of the maximum and minimum value of the streamfunction. These extrema occur at the centre of the two recirculations established about the axial mid−plane of the cavity (z*/s = ½). In Fig. 2 the stronger recirculation is nearer the left−hand disc and there is a stagnation point on the left−hand disc in the inner part of the cavity, The periodic variation is between this structure and the mirror−image situation, where the stronger recirculation is closer to the right−hand disc. The situation shown in Fig. 2 corresponds to the peak of the streamfunction values in Fig. 3. (The secondary peaks seen in the streamfunction variations were found to reduce when smaller time steps were used, however the other features of the solution were not affected).

Fig. 4 shows the computed tangential velocity on the mid−plane between the discs (z*/s = ½). The axes are chosen to illustrate the approach to Rankine (combined free and forced) vortex behaviour in the flow (see Owen and Rogers, 1995), since for such a flow:

$$V_\phi = C / r^* + Dr^* \quad => \quad V_\phi / \Omega r^* = A\, r^{-2} + B \qquad (5)$$

where A and B are constants (different for each test condition).

The standard deviation S plotted in Fig. 4 shows that there is little effect of unsteadiness on the mid−plane tangential velocity. The time−averaged velocity distribution is in good agreement with a steady axisymmetric laminar flow computation performed by Lewis et al (1997), except in the lower part of the

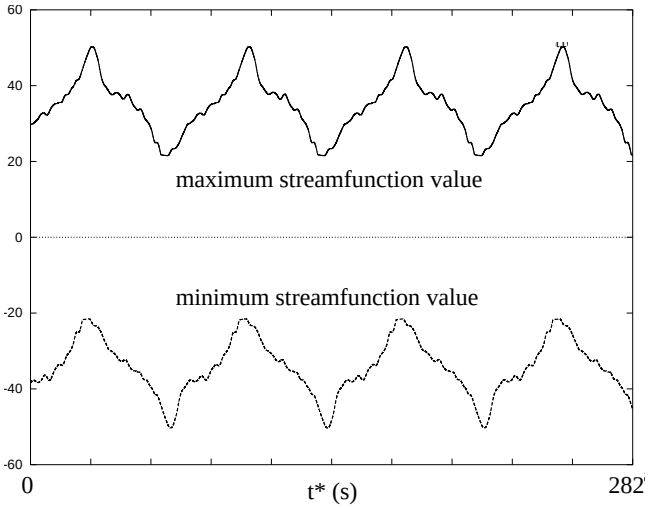

Fig. 3 Streamfunction time−history: $Re_\phi = 10^4$, G = 0.3

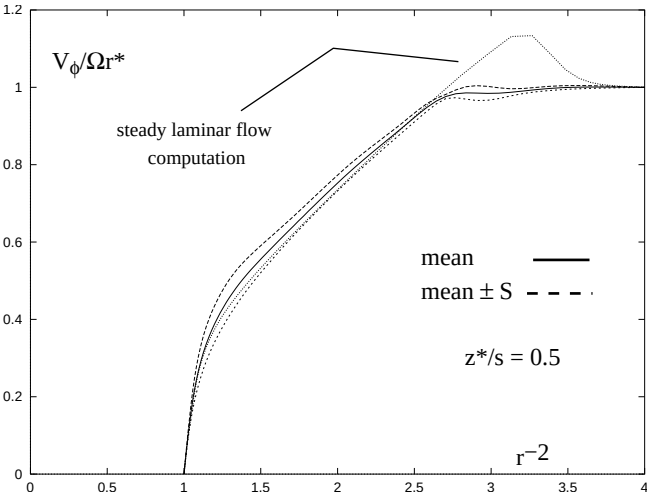

Fig. 4 Time−averaged tangential velocity distribution and comparison with steady laminar flow computation: $Re_\phi = 10^4$, G = 0.3

system ($r^{-2} > 2.5 \Rightarrow r < 0.65$ approx.): in the unsteady computation, solid body rotation occurs in this region. The symmetric recirculations obtained for the steady flow computation are those shown in Fig. 1.

4 RESULTS FOR $Re_\phi = 1.46 \times 10^5$, G = 0.3

This case was selected for computation as it was the lowest rotational Reynolds number for which experimental velocity data were obtained in the study reported by Gan et al (1996). For numerical stability, a 97 x 129 grid and non−dimensional time step $\Delta t = 0.355 \times 10^{-7}$ were required. The calculation time for 200,000 time steps (to t* = 56.s) was around 24 CPU hours on a single processor of a Silicon Graphics Power Challenge machine.

Unlike the case at $Re_\phi = 10^4$ described above, the computation at $Re_\phi = 1.46 \times 10^5$ gave rise to an unsteady solution which was not periodic. Fig. 5 shows instantaneous computed flowfields for this case for t* = 22.5 s and t* = 28.2 s, and the time−history of the streamfunction extrema in this interval is shown in Fig. 6.

Fig. 5a shows a secondary flow structure based on a system of two principal recirculations, similar to that obtained for $Re_\phi = 10^4$ (Fig. 2) but with greater variation of inward penetration with time. Fig. 5b shows contours of non−dimenisonal tangential velocity, v, at the corresponding times. The axial distribution of tangential velocity is roughly uniform outside the thin boundary layers on the discs, except close to the mid−plane where high angular−momentum fluid is convected inwards from the boundary layers meeting on the stationary casing.

Fig. 7 shows the good agreement obtained between the time−averaged tangential velocities for the unsteady computation and experimental data from the study described by Gan et al (1996). The data is consistent with Rankine vortex flow. An axisymmetric steady computation, carried out using the low Reynolds number two equation turbulence model of Launder and Sharma (1974), failed to reproduce this behaviour and is in poor agreement with the data. (Mirzaee et al (1997) found the turbulence model to be deficient for this flow. The model is able to represent transition from laminar to turbulent flow, and the results suggest that low turbulence levels occur in this case. Computations carried out by Mirzaee (1997) assuming steady laminar flow were in slightly less good agreement with the data.)

Wilson et al (1997) also compared the results of the unsteady computation described here with LDA data for the axial distribution of radial velocity at two radial locations. The computed time−averaged distributions were in reasonably good agreement with the data, however the large standard deviation about the computed mean value (as suggested by the results shown in Fig. 5) was not confirmed by similar unsteadiness in the experimental observations. Three−dimensional computations may be required to capture more accurately the behaviour of this flow.

Computations were also attempted for $Re_\phi = 3.75 \times 10^5$ and G = 0.3, where experimental data were also available. However, reliable results could not be obtained for grid resolutions up to 144 x 176. Results were obtained at a similar rotational Reynolds and a narrower gap ratio G = 0.05, for which sufficient resolution in the centre of the cavity was possible without computation times becoming excessive. The results of this calculation are described below.

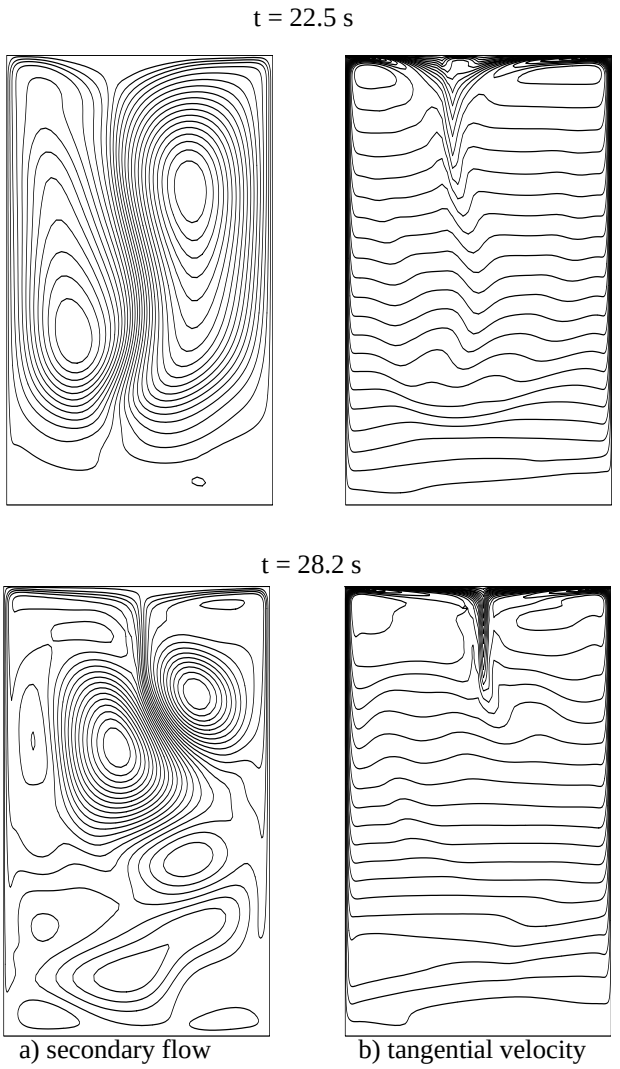

Fig. 5 Instantaneous computed flowfields: $Re_\phi = 1.46 \times 10^5$, G = 0.3

5 RESULTS FOR $Re_\phi = 4.5 \times 10^5$, G = 0.05

This case was studied experimentally by Abrahamson et al (1989). In the present work, computations were performed on a 64 x 128 nonuniform grid with a non−dimensional time step $\Delta t = 0.2 \times 10^{-7}$ (for convenience, b = 0.382 m was used as above, though this did not match the value for the experiment).

Instantaneous computed streamlines, shown in Fig. 8a−c, again show two principal recirculations, in the outer part of the cavity, affecting the radial inflow between the discs. The inflow was directed more toward the left or right hand disc at different times, depending on the relative size of the recirculating regions near the outer casing. Fig. 9 shows the behaviour of the streamfunction extrema with time for the entire computation (16.8 s, requiring 150,000 time steps), and Fig. 10 shows the time−averaged mid−plane tangential velocity distribution in comparison with the measured data. There is solid body rotation in the inner part of the system, extending to around r = 0.8 for the computations. The measurements, inferred from flow visualisations by Abrahamson et al (1989) and digitised here from the results presented, suggest further inward penetration of the recirculating flow than was predicted, either in this unsteady calculation or in a steady turbulent computation carried out for this case by Mirzaee (1997). As for the case described above, three−dimensional calculations are required to identify the possible restrictiveness of the axisymmetric assumption, and the importance of the vortical structures observed and secribed by Abrahamson et al on the development of the flow.

6 CONCLUSIONS AND FUTURE WORK

Axisymmetric computations have been carried out for unsteady flow in a rotating cavity with a stationary outer casing, for rotational Reynolds numbers between 10^4 and 4.5×10^5. Reasonable agreement has been obtained between time−averaged results and experimental data for tangential velocity distributions, which follow a Rankine vortex structure. Three dimensional computations are required to confirm the unsteady behaviour of the

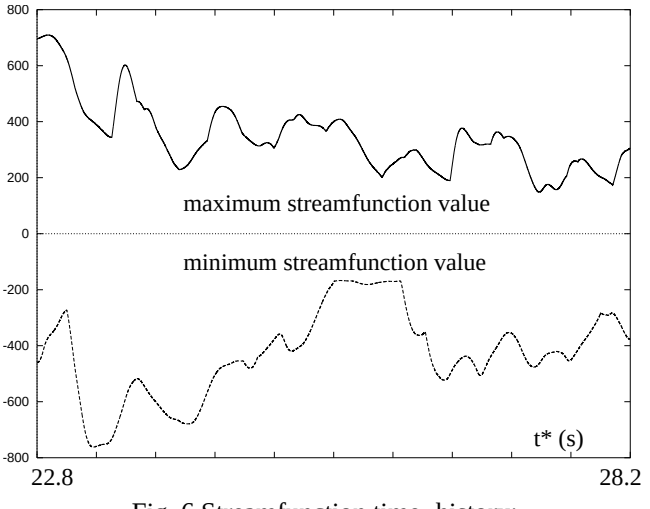

Fig. 6 Streamfunction time−history: $Re_\phi = 1.46 \times 10^5$, G = 0.3

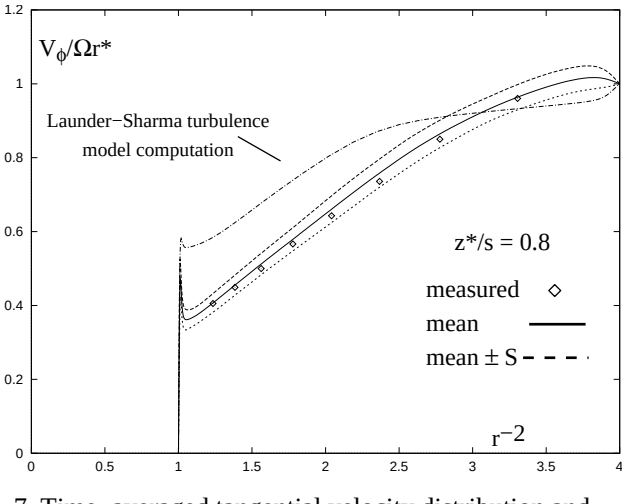

Fig. 7 Time−averaged tangential velocity distribution and comparison with experimental data: $Re_\phi = 1.46 \times 10^5$, G = 0.3

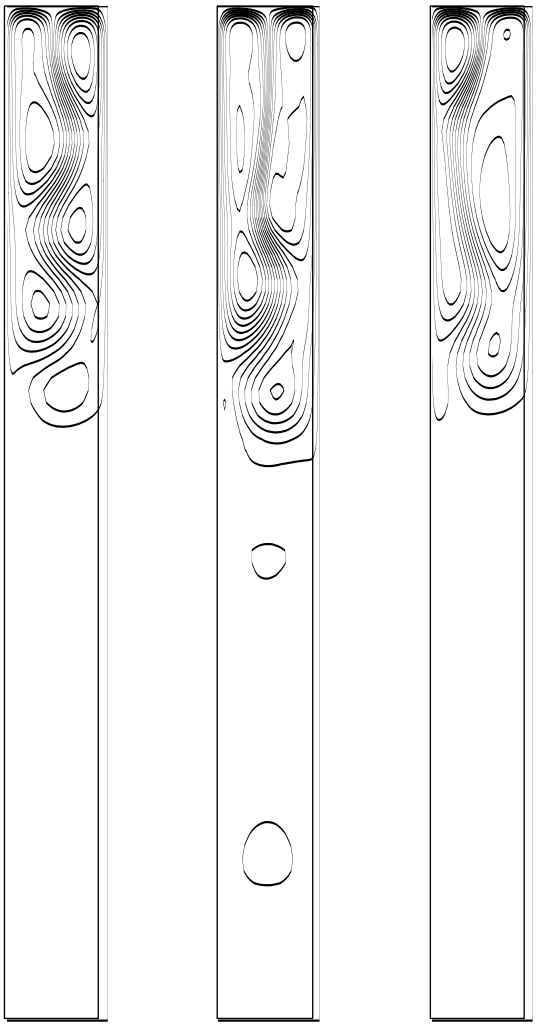

a) t* = 5.6 s b) t* = 11.2 s c) t* = 16.8 s

Fig. 8 Instantaneous computed secondary flow streamlines: $Re_\phi = 4.5 \times 10^5$, G = 0.05

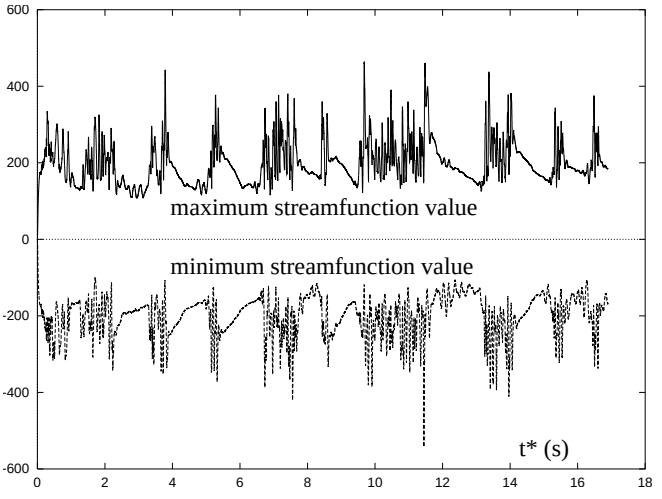

Fig. 9 Streamfunction time−history: $Re_\phi = 4.5 \times 10^5$, G = 0.05

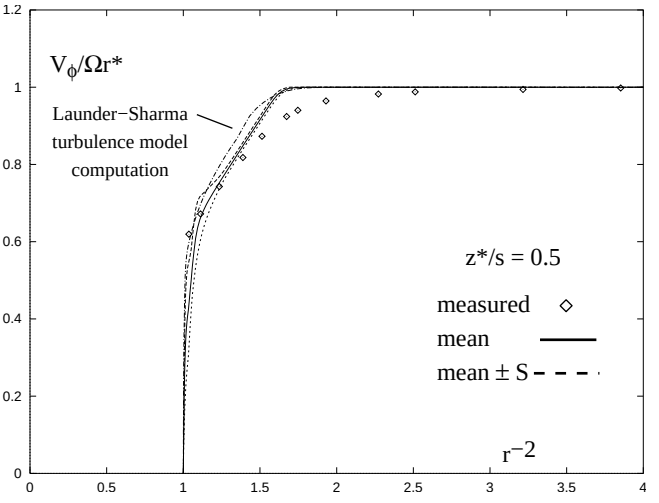

Fig. 10 Time−averaged tangential velocity distribution and comparison with experimental data: $Re_\phi = 4.5 \times 10^5$, G = 0.05

secondary flows, and to allow the parametric effects of rotational Reynolds number and gap ratio to be studied with greater confidence.

NOMENCLATURE

a, b	inner, outer radius of disc
G	gap ratio (= s/b)
k	turbulent kinetic energy
r , ϕ , z	radial, tangential, and axial coordinates
Re_ϕ	rotational Reynolds number (= $\rho\Omega b^2/\mu$)
s	axial gap between discs
S	standard deviation
t	time
u , w	radial, axial velocity
v	tangential velocity in a rotating frame
V_ϕ	tangential velocity in the stationary frame
∇^2	Laplace operator (= $(1/r)\partial(r\partial/\partial r)/\partial r + \partial^2/\partial z^2$)
ψ	streamfunction (u,w) = ($(1/r)\partial\psi/\partial z$, $-(1/r)\partial\psi/\partial r$)
Δt	non−dimensional solution time step (= $\nu\Delta t^*/b^2$)
ε	turbulent energy dissipation rate
ν	kinematic viscosity (for air, $\nu = 1.84 \times 10^{-5}$ m^2/s)
Φ	re−scaled streamfunction ($\psi = r\Phi$)
ω	vorticity ($\omega = \partial u/\partial z - \partial w/\partial r$)
Ω	angular speed of discs

superscripts

*	dimensional value (see equation (3))

REFERENCES

Abrahamson, S. D., Eaton, J. K. and Koga, D. J. 1989 The flow between shrouded co−rotating discs, Physics of Fluids, vol. 1, no. 2, pp 241−251

Chang, C. J., Humphrey, J. A. C. and Greof, R. 1990 Calculation of turbulent convection between co−rotating discs in axisymmetric enclosures, Int. J. Heat and Mass Transfer, vol. 33, no. 12, pp 2701−2729

Gan, X., Mirzaee, I., Owen, J. M., Rees, D. A. S. and Wilson, M. 1996 Flow in a rotating cavity with a peripheral inlet and outlet of cooling air, ASME Int. Gas Turbine and

Aeroengine Cong., Birmingham, paper 96−GT−309
Launder, B. E. and Sharma, B. I. 1974 Application of the energy dissipation model of turbulence to flow near a spinning disc, Letters in Heat and Mass Transfer, v 1, 131−138

Lewis, T. W., Wilson, M. and Rees, D. A. S. 1997 Unsteady laminar flow and heat transfer in a rotating cavity with a stationary outer surface, to be presented at 11th International Heat Transfer Conference, Kyongju, Korea, August

Mirzaee, I. 1997 Computation of flow and heat transfer in a rotating cavity with peripheral inflow and outflow of cooling air, PhD thesis, University of Bath
Mirzaee, I., Gan, X., Wilson, M. and Owen, J. M. 1997 Heat transfer in a rotating cavity with a peripheral inflow and outflow of cooling air, ASME Int. Gas Turbine and Aeroengine Cong., Orlando, paper 97−GT−136

Owen, J.M. and Rogers, R.H. 1995, Flow and heat transfer in rotating disc systems: Vol. 2, Rotating cavities [Research Studies Press, Taunton, UK and John Wiley, NY, USA]

Wilson, M., Arnold, P. D., Lewis, T. W., Mirzaee, I., Rees, D. A. S. and Owen, J. M. 1997 Instability of flow and heat transfer in a rotating cavity with a stationary outer casing, Eurotherm 55 (Heat Transfer in Single Phase Flow), Santorini, Greece, September